A simplified design for maximum thrust in non-saturation region of double-sided transverse flux PMLSM

Jung-Seob Shin [a], Takafumi Koseki [a],

[a] Department of Electrical Engineering, The University of Tokyo, Tokyo 113-8656, Japan

jungseobshin1008@koseki.t.u-tokyo.ac.jp

***Abstract* — Large thrust is one of the performance requirements for the permanent magnet linear synchronous motor (PMLSM). In this paper, we propose a simplified design method for maximum thrust in non-saturation region of double-sided transverse flux PMLSM. The usefulness of the proposed method are analyzed and evaluated by using a 3D finite element method.**

***Keywords* — Equivalent reluctance network method, 3-D finite element method, thrust design.**

I. Introduction

Large thrust is one of the performance requirements for the permanent magnet linear synchronous motor (PMLSM). The transverse-flux machinery (TFM) is suitable for a large-thrust design [1]. However, the manufacturing process for conventional TFMs is difficult because of the complex structure resulting from the 3D magnetic circuit [2], [3]. In the conventional manufacturing process, a large number of segmented components are needed to make up the magnetic circuit, and the use of lamination is difficult.

On the other hand, the estimation of the design point at which maximum thrust is obtained is important in the preliminary design stage because it saves design time. In a previous study, we proposed a double-sided transverse flux linear synchronous motor to address the problem of the complex structure in TFM and a theoretical design of thrust for a simple estimation [4]. It proved useful for finding the maximum thrust under a condition in which only the structure and total volume are known. However, the method is not effective when magnetic saturation occurs because of the linear characteristic between the thrust and current. If the design point from the previous study is positioned in the saturation region where there is a non-linear characteristic between thrust and current, losses increase and control performance deteriorates, which degrades motor performance [5], [6]. Therefore, it is important to estimate the flux related to magnetic saturation and its position and develop a design for maximizing thrust in the range where magnetic saturation does not occur.

In this paper, we propose a simplified design method for maximum thrust in non-saturation region in the preliminary design stage. In Section II, operational principle of the double-sided transverse flux PMLSM proposed in the previous study used in thrust design is introduced. In Section III, a simplified design for maximum thrust in a non-saturation region is described. Finally, in Section IV, the usefulness of the proposed method is analyzed and evaluated by 3D finite element method (FEM).

II. Operational Principle of the Proposed Model Used in Thrust Design

Fig. 1 shows the basic configuration of the proposed model which is used in thrust design.

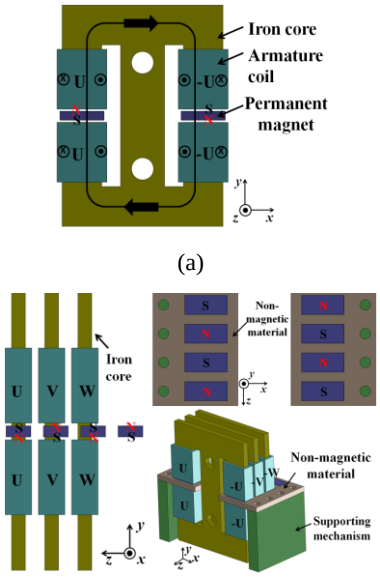

Fig. 1. The basic configuration of the three-phase unit. (a) Armature and field units. (b) Configuration along the moving direction. (In (a), black arrows denote flux flow under a no-load condition. In (b), −U, −V, and −W are present components shifted by 180 degrees from U, V, and W.)

The armature unit—which is the mover—consists of an iron core and four coils; the field unit—which is the stator—consists of two magnets. The two coils on the left side are wound in a direction opposite to those on the right side, and these coils are connected in series, as shown in Fig. 1(a). Armature cores and magnets are arranged along the moving direction *z*, as shown in Fig. 1(b). Each core is spatially separated by 120 degrees difference. Field magnets are fixed in a non-magnetic material plate and each magnet is electrically separated

by 180 degrees. By applying AC current with 120-degree phase difference to armature coil, the proposed model operates as a 3-phase AC synchronous motor.

Unlike the configuration in conventional TFM, the proposed model has a 2D magnetic circuit in which the main flux from the north pole flows transversely to the south pole along an armature core, as shown in Fig. 1(a). This magnetic circuit eases manufacturing because of the following reasons:

(a) Simple structure: Only two magnets and one armature core, which is not segmented, are required to construct the magnetic circuit.

(b) Use of lamination: The iron core is easily fabricated using laminated steel plates.

(c) Small sensitivity of normal attractive force to assembly error: It has been reported that normal attractive force reaches the same level as that of thrust with an air gap imbalance of only 0.5 mm, resulting from the use of two independent magnetic circuits in a conventional double-sided configuration [7]. However, in the proposed model, the magnetic circuit is not independent and mainly changes irrespective of whether there is an air gap imbalance because the total magnetic air gap is constant. Thus, the burden placed on the supporting mechanism is small, and manufacture is easy.

III. The Simplified Design for Maximum Thrust in Non-saturation Region

A. Specification and Materials in the Proposed Design

We focused on the thrust in a one-phase configuration because thrust in a three-phase configuration can be estimated from the results obtained in the one-phase configuration. All dimensions, except for l_a, l_c, and l_m, are fixed and are selected on the basis of spatial limitations. A total volume of 80 mm × 100 mm × 27 mm and three-core/two-pole combination were selected. In this volume, the pole pitch, τ_p, and slot pitch, τ_s, are 13.5 and 9 mm, respectively. In Fig. 3, 1.5 T denotes the maximum flux density in the non-saturation region [8].

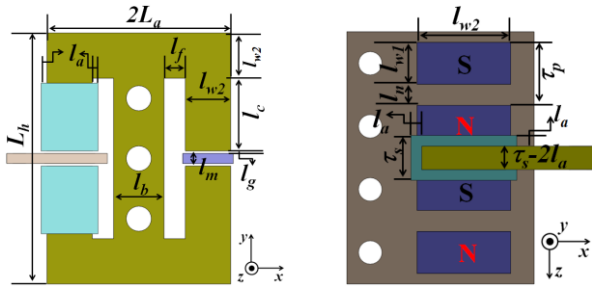

(a) (b)

Fig. 2. Specifications of parts. (a) *x*–*y* plane. (b) *x*–*z* plane. (In (a), armature coils and non-magnetic material on the right side are removed for clarity.)

TABLE I
DESIGN SPECIFICATIONS AND MATERIALS [8]-[9]

Symbol	Quantity	Symbol	Quantity	Symbol	Quantity
L_a [mm]	40	l_f [mm]	10	l_g [mm]	1
L_h [mm]	100	l_b [mm]	20	l_n [mm]	2
τ_p [mm]	13.5	l_{w1} [mm]	11.5	l_a, l_m l_c [mm]	Variables
τ_s [mm]	9	l_{w2} [mm]	20		

Materials	Note	Materials	Note
50JN230	Iron core	N50M	Magnet (NdFeB,Br:1.4T)

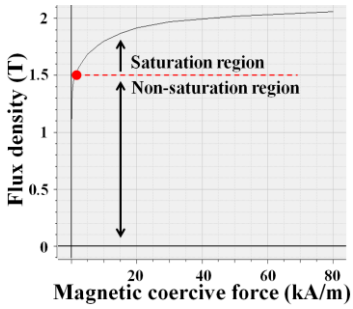

Fig. 3. *B*—*H* characteristic of 50JN230.

B. Key Design Variables in the Proposed Design

Key design variables are l_a, l_c, and l_m. Variables l_a and l_c denote the half slot length in the moving direction and the height in the space in which the armature coil is wound, respectively. They are related to the electric load, *NI*, which represents the magnetomotive force (MMF) on the armature side. It depends on the space in the total volume and is expressed as (1). In (1), $N(l_a, l_c)$ is the number of windings per armature pole; I is armature current; α is packing factor of coil; A_w (l_a, l_c) is the cross-section area where the armature coil is wound; S_c is dimension of the armature coil; and J is current density. From (1), $N(l_a, l_c)$ is proportional to l_a and l_c.

$$N(l_a,l_c)I = \frac{\alpha A_w(l_a,l_c)I}{S_c} = \alpha A_w(l_a,l_c)J \quad \left(A_w(l_a,l_c) = l_a \times l_c\right) \tag{1}$$

The term l_a affects the width, l_z, and cross-section, A_a, of the armature core, as expressed in (2). $A_a(l_a)$ is inversely proportional to $N(l_a, l_c)$ under the same τ_s.

$$A_a(l_a) = l_z(l_a) \times l_{w2} \qquad (l_z(l_a) = \tau_s - 2l_a) \tag{2}$$

The variable l_m is the magnet length in the magnetization direction. It is related to the magnetic load that represents the MMF of the field magnet, depends on the space of the total volume, and is expressed as $H_c l_m$. The relation between l_m and l_c is given in (3). From (1) and (3), $N(l_a, l_c)$ is inversely proportional to $H_c l_m$ under the same l_a.

$$l_m = L_h - 2(l_g + l_c + l_{w2}) \tag{3}$$

C. Simple Estimation of Maximum Flux in the Armature Core by Armature reaction and its Position

Whether the design point is in non-saturation region or not depends on the maximum flux in the armature core, and the amount of the flux depends on magnetic and electric loads. When sinusoidal current is applied to the armature coil under a condition in which the *d*-axis current is maintained at zero, flux distribution in the armature core due to armature reaction is as illustrated in Fig. 4.

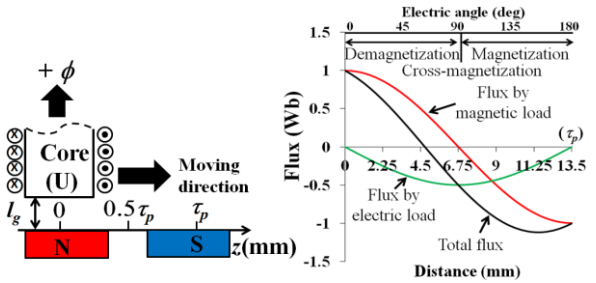

Fig. 4. Flux distribution in the armature core due to armature reaction. (The positive value on the left side represents the direction in which the flux flows into the iron core.)

When z is equal to 0, the total flux is equal to the flux generated by the magnetic load because the armature current is equal to zero. When the armature core is between zero and 0.5 τ_p, the total flux decreases because of demagnetization. When z is equal to 0.5 τ_p, the total flux in the iron core is equal to the flux generated by the electric load. This is because of cross-magnetization. When the armature core is between 0.5 τ_p and τ_p, the total flux increases because of magnetization. If magnetic saturation is negligible, nonlinear characteristics in saturation region is also negligible. Therefore, the total flux is calculated by the principle of superposition, as expressed in (4). In (4), ϕ_{tl}, ϕ_{ml}, and ϕ_{el} denote total flux and the flux generated by the magnetic and electric loads. Also, ϕ_{ml_max} and ϕ_{el_max} denote the maximum values generated by both loads at z = 0 and 0.5 τ_p, where both loads affect ϕ_{tl} independently.

$$\phi_{tl}(z) = \phi_{ml}(z) - \phi_{el}(z) = \phi_{ml\_\max}\cos\left(\frac{\pi z}{\tau_p}\right) - \phi_{el\_\max}\sin\left(\frac{\pi z}{\tau_p}\right) \quad (4)$$

Only one maximum point exists between 0 and τ_p. The position of the point $z_{\_max}$ is obtained, expressed as (5). The flux density in the armature core in this position, B_{max}, is calculated by (6). One necessary condition to avoid magnetic saturation is that B_{max} must be lower than 1.5 T.

$$\frac{d\phi_{tl}(z)}{dz} = 0 \rightarrow z_{\_\max} = \frac{\tau_p}{\pi}\tan^{-1}(-A) + \tau_p \quad \left(A = \frac{\phi_{el\_\max}}{\phi_{ml\_\max}}\right) \quad (5)$$

$$B_{\max} = \frac{\phi_{tl}(z_{\max})}{A_a(l_a)} \quad (6)$$

The term $z_{\_max}$ depends on the ratio of the flux generated by electric and magnetic loads, A, as shown in Fig. 5. The position of the maximum point approaches from τ_p to 0.5 τ_p with increase in A. The total flux at $z_{\_max}$ is greater than ϕ_{ml_max}, in all the range of A. Another necessary condition to avoid magnetic saturation is that the flux density in the armature core at z = 0 must be lower than 1.5 T. The behavior in V and W phases is the same as that in the U phase, except for $z_{\_max}$.

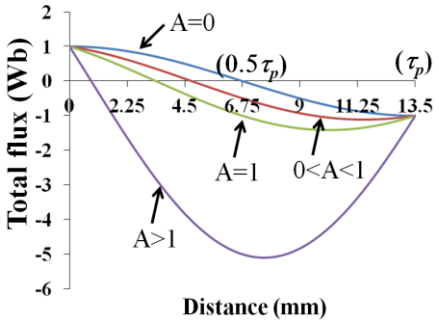

Fig. 5. Total flux distribution by the flux ratio A.

If B_{max} is larger than 1.5 T at certain design point, it means that the design point is in the saturation region. Hence, there exist differences between theoretical values based on the principle of superposition and real values due to nonlinear characteristics in saturation region. However, an exact value in saturation region is not important in the proposed design because B_{max} are only used to confirm whether the design point is in saturation region or not.

D. Calculation of ϕ_{ml_max} and ϕ_{el_max}

The equivalent reluctance network (ERN) method has been employed for the calculation of ϕ_{ml_max} and ϕ_{el_max} because it offers the advantage of a very short computation time [6], [10]. Fig. 6 shows magnetic circuit models.

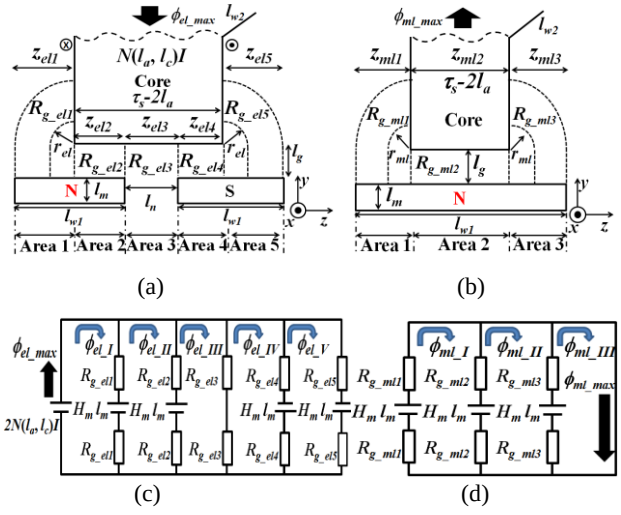

Fig. 6. Magnetic circuit models for flux calculation by electric and magnetic loads. (a) Model at z = 0.5 τ_p. (b) Model at z = 0. (c) Equivalent magnetic circuit at z = 0.5 τ_p. (d) Equivalent magnetic circuit at z = 0. (Only a half model is illustrated because of the symmetric structure.)

We have employed a 2D ERN method to facilitate simple calculation. The models and each reluctance component used in our calculation are linear and have been determined on the basis of [6], [10]. In Fig. 6, z is the width of each area; R_g is the magnetic reluctance in the air; and H_m is the magnetic-field component of the magnet at the operating point. The components related to ϕ_{el_max} and ϕ_{ml_max} are ϕ_{el_I} and ϕ_{ml_III}, respectively. They are calculated from (7) to (13), where $\phi_{\_j}$, R_{g_j}, and $M_{\_j}$ are flux, magnetic reluctance, and MMF matrices, respectively.

$$\phi_{\_j} = R_{g\_j}^{-1} \times M_{\_j} \quad (j = el, ml) \tag{7}$$

$$\phi_{\_el} = \left[\phi_{el\_I}, \phi_{el\_II}, \phi_{el\_III}, \phi_{el\_IV}, \phi_{el\_V}\right]^T \tag{8}$$

$$\phi_{\_ml} = \left[\phi_{ml\_I}, \phi_{ml\_II}, \phi_{ml\_III}\right]^T \tag{9}$$

$$R_{g\_el} = \begin{bmatrix} 2R_{g\_el1} & -2R_{g\_el1} & 0 & 0 & 0 \\ -2R_{g\_el1} & 2R_{g\_el2}+2R_{g\_el3} & -2R_{g\_el2} & 0 & 0 \\ 0 & -2R_{g\_el2} & 2R_{g\_el2}+2R_{g\_el3} & -2R_{g\_el3} & 0 \\ 0 & 0 & -2R_{g\_el3} & 2R_{g\_el3}+2R_{g\_el4} & -2R_{g\_el4} \\ 0 & 0 & 0 & -2R_{g\_el4} & 2R_{g\_el4}+2R_{g\_el5} \end{bmatrix} \tag{10}$$

$$R_{g\_ml} = \begin{bmatrix} 2R_{g\_ml1}+2R_{g\_ml2} & -2R_{g\_ml2} & 0 \\ -2R_{g\_ml2} & 2R_{g\_ml2}+2R_{g\_ml3} & -2R_{g\_ml3} \\ 0 & -2R_{g\_ml3} & 2R_{g\_ml3} \end{bmatrix} \tag{11}$$

$$M_{\_el} = \left[2N(l_a, l_c)I - H_m l_m, 0, H_m l_m, H_m l_m, 0\right]^T \tag{12}$$

$$M_{\_ml} = \left[0, 0, H_m l_m\right]^T \tag{13}$$

E. Process of Thrust Calculation

Because thrust depends on electric and magnetic loads and these loads are determined by l_a and l_m, we have focused on l_a and l_m. Below is the process of thrust calculation.

(a) Determine constrains on l_a and l_m
(b) Calculate ϕ_{el_max}, and ϕ_{ml_max} at $z = 0, 0.5\tau_p$ from (7)
(c) Calculate $z_{\_max}$ from (5)
(d) Calculate ϕ_{tl} ($z_{\_max}$) and B_{max} from (4) and (6)
(e) Find the design point at which B_{max} is less than 1.5T
(f) Calculate the thrust per phase F_{t_max} in the design point

The selected design point in (e) is the optimal design point, and F_{t_max} is the maximum thrust in non-saturation region. It is expressed as (14) by substituting ϕ_{ml_max} for flux in the armature core under a no-load condition as shown in [4].

$$F_{t\_\max} = p\frac{E_{rms}I}{v} = \frac{\sqrt{2}p\pi\phi_{ml\_\max}N(l_a, l_c)I}{2\tau_p} \tag{14}$$

IV. Analysis and Evaluation Using 3D FEM

Table II and Fig. 7 show the specifications in analysis and results from both theoretical and 3D FEM analyses. The JMAG-Designer 10.4.3h commercial package was used for the 3D FEM analysis [11], whose feasibility has been experimentally proven in [12]. There is a good agreement between theoretical values based on the 2D ERN method and 3D FEM values.

The amount by which ϕ_{ml_max} decreased and that by which ϕ_{el_max} increased with increase in l_a, resulting from decrease in the cross-section of the armature core and increase in electric load are shown in Fig. 7(a). Hence, the ratio of the flux generated by electric and magnetic loads, A, increased, as shown in Fig. 7(b). However, A was lower than 1 in all cases of l_a, which means that the total flux in this condition was affected by ϕ_{ml_max} rather than by ϕ_{el_max}. Hence, total flux decreased when l_a increased, as shown in Fig. 7(c). On the other hand, B_{max} increased with l_a because of the decreased cross-section of the armature core, as shown in Fig. 7(d).

The optimal design point was approximately equal to, but below, l_a = 2.625 mm, as shown in Fig. 7(d). Above l_a = 2.625 mm, where the theoretical value of B_{max} was over 1.5 T, there are differences between theoretical and 3D FEM values because the iron core starts to saturate. Therefore, we decided to use the optimal design point as l_a=2.5 mm, considering the thickness of the iron core, which was 0.5 mm [8].

The theoretical value of F_{t_max} at this point was 37.2 N, almost the same as the 3D FEM value as shown in Table III. The armature core width l_z was 4 mm, and the number of winding turns per armature pole was 73 turns.

TABLE II
Specifications in Analysis

Symbol	Quantity	Symbol	Quantity
J [A/mm^2]	7	α	0.7
I [A]	4.5	v [m/s]	1
l_a [mm]	1 ~ 3	l_m [mm]	4

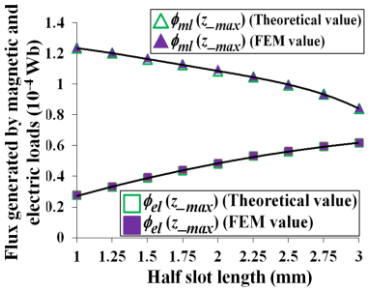

(a)

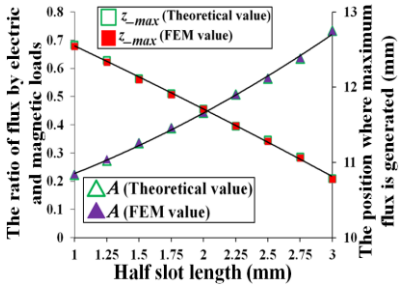

(b)

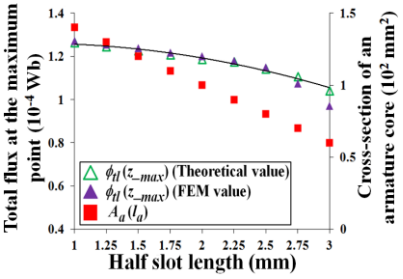

(c)

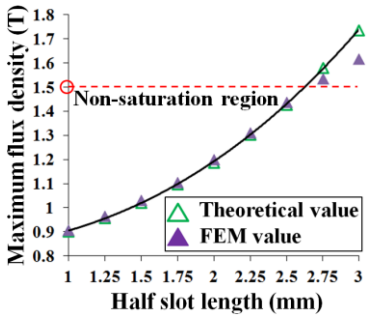

(d)

Fig. 7. Theoretical and 3D FEM results. (a) ϕ_{ml_max} and ϕ_{el_max}. (b) A and $z_{\_max}$. (c) ϕ_{tl} ($z_{\_max}$) and A_a (l_a). (d) B_{max}.

TABLE III
RESULTS OF THRUST AT THE OPTIMAL POINT

F_{t_max} (Theoretical value) [N]	F_{t_max} (3D FEM value) [N]
37.2	38.8

V. CONCLUSION

In this paper, a design method for the maximum thrust in non-saturation region of a double-sided transverse flux PMLSM was proposed as a simple design method in the preliminary design stage. In the process of the optimal design for maximum thrust in non-saturation region, it is important to confirm whether certain design point is in saturation region or not. This is determined by the maximum flux at certain design point and it is affected by electric and magnetic loads at that point. In the proposed method, the maximum flux and its position, the optimal point, and thrust at the point is simply estimated from flux calculations at only $z = 0$ and $0.5\,\tau_p$, using a 2D ERN method. Also, there is a good agreement between theoretical and 3D FEM values. Therefore, the proposed method is useful as a simple design method for maximum thrust in the preliminary stage.

Future studies will involve further analysis of the prototype model through experimental verification, including thrust, thrust ripple, and positioning accuracy.

ACKNOWLEDGEMENT

We wish to acknowledge the assistance and support of the preparing group for the student sessions of the SNU-UT Joint Seminar 2013.

REFERENCE

[1] H. Weh, "Permanenterregte Synchronmaschine hoher Kraftdichte nach dem Transversalflusskonzept," *etzArchiv*, vol. 10, pp. 143–149, 1988.

[2] S. D. Joao and V. Mauricio, "Transverse flux machine: what for?," *IEEE Multidisciplinary Engineering Education Magazine*, vol. 2, no. 1, pp. 4–6, 2007.

[3] M. Zhao, Q. Wang, J. Zou, and G. Wu, "Development and analysis of tubular transverse flux machine with permanent-magnet excitation," *IEEE Trans. Ind. Elect.*, vol. 59, no. 5, pp. 2198–2207, 2012.

[4] J. S. Shin, T. Koseki, and H. J. Kim, "Proposal and design of short armature core double-sided transverse flux type linear synchronous motor," *IEEE Trans. Magn.*, vol. 48, no. 11, pp. 3871–3874, 2012.

[5] M. Siatkowski and B. Orlik, "Influence of Saturation Effects in a Transverse Flux Machine," *the 13th Power Electronics and Motion Control Conference, EPE-PEMC*, pp. 830–836, 2008.

[6] H. Polinder, J. G. Slootweg, M. J. Hoeijmakers, and J. C. Compter, "Modeling of a Linear PM Machine Including Magnetic Saturation and End Effects: Maximum Force-to-Current Ratio," *IEEE Trans. Magn.*, vol. 39, no. 6, pp. 1681–1688, 2003.

[7] Y. Misawa, S. Sugita, and S. Onodera, "Linear servo motor: double-sided core type model," *SANYO DENKI Technical Report*, no. 15, pp. 25–27, 2003, written in Japanese.

[8] JFE Steel Corp., http://www.jfe-steel.co.jp/.

[9] Shin-EtsuChemicalCo.,Ltd., http://www.shinetsu.co.jp/j/index.shtml.

[10] B. Sheikh-Ghalavand, S. Vaez-Zadeh, and A. Hassanpour Isfahani, "An Improved Magnetic Equivalent Circuit Model for Iron-Core Linear Permanent-Magnet Synchronous Motors," *IEEE Trans. Magn.*, vol. 46, no. 1, pp. 112–120, 2010.

[11] JSOL Corp., http://www.jmag-international.com/.

[12] T. Nakamura, T. Koseki, and Y. Aoyama, "A low-speed high-torque permanent magnet synchronous motor – Reducing cogging torque and eddy current loss –", *The Japanese Society of Applied Electromagnetics and Mechanics*, vol. 20, no. 2, pp.410–415, 2012.